

Robust Cross-domain CT Image Reconstruction via Bayesian Noise Uncertainty Alignment

Kecheng Chen, Haoliang Li, Renjie Wan, Hong Yan, *Fellow, IEEE*

Abstract—In this work, we tackle the problem of robust computed tomography (CT) reconstruction issue under a cross-domain scenario, *i.e.*, the training CT data as the source domain and the testing CT data as the target domain are collected from different anatomical regions. Due to the mismatches of the scan region and corresponding scan protocols, there is usually a difference of noise distributions between source and target domains (*a.k.a.* noise distribution shifts), resulting in a catastrophic deterioration of the reconstruction performance on target domain. To render a robust cross-domain CT reconstruction performance, instead of using deterministic models (*e.g.*, convolutional neural network), a Bayesian-endowed probabilistic framework is introduced into robust cross-domain CT reconstruction task due to its impressive robustness. Under this probabilistic framework, we propose to alleviate the noise distribution shifts between source and target domains via implicit noise modeling schemes in the latent space and image space, respectively. Specifically, a novel Bayesian noise uncertainty alignment (BNUA) method is proposed to conduct implicit noise distribution modeling and alignment in the latent space. Moreover, an adversarial learning manner is imposed to reduce the discrepancy of noise distribution between two domains in the image space via a novel residual distribution alignment (RDA). Extensive experiments on the head and abdomen scans show that our proposed method can achieve a better performance of robust cross-domain CT reconstruction than existing approaches in terms of both quantitative and qualitative results.

Index Terms—Robust CT reconstruction, probabilistic model, noise modeling, adversarial learning

I. INTRODUCTION

LOW-dose computed tomography (LDCT) image reconstruction is a very popular research orientation recently. Usually, researchers aim to reconstruct potential normal-dose CT (NDCT) images from LDCT images based on the image domain [1], projection domain [2], or dual domains [3]. This is highly beneficial to the patients and radiologists. On the one hand, compared with NDCT imaging mode, the patients, especially for the children, will suffer from lower radiation risk under the LDCT imaging mode [4]. On the other hand, by the virtue of LDCT image reconstruction technique, it is sufficient for the radiologists to leverage reconstructed LDCT images with reduced noise to make clinical decisions. Among various approaches, deep learning (DL)-based LDCT reconstruction methods are dominant recently [5], due to their impressive

This work is supported by the Hong Kong Innovation and Technology Commission (InnoHK Project CIMDA).

K. Chen, H. Li, and H. Yan are with the Department of Electrical Engineering and the Center for Intelligent Multidimensional Data Analysis, City University of Hong Kong, Hong Kong, China. (e-mail: cs.ckc96@gmail.com; haoliang.li@cityu.edu.hk; h.yan@cityu.edu.hk)

R. Wan is with the Department of Computer Science, Hong Kong Baptist University, Hong Kong, China. (e-mail: wanpeoplejie@gmail.com)

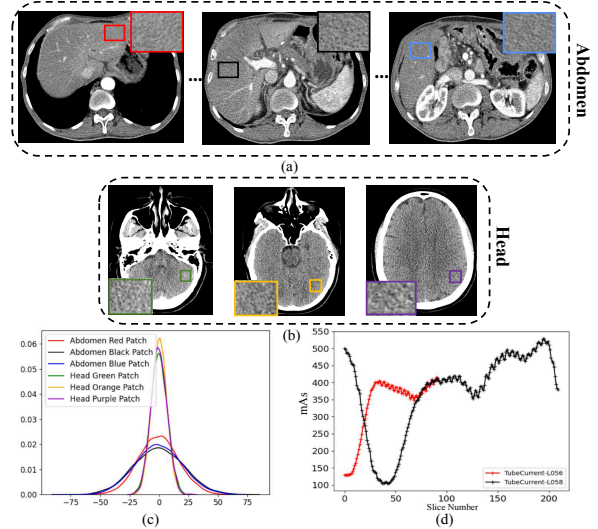


Fig. 1. Examples of head and abdomen scans. (a) Abdomen LDCT scans. (b) Head LDCT scans. (c) Probability density functions of noise distributions (the subtraction of the LDCT image from the NDCT image) in selected ROIs from (a) and (b), (d) Illustration of dynamic changes of CT scan protocol (*i.e.*, mAs) in two different patients with abdomen scans.

capacities of noise suppression and structural information retaining. By utilizing LDCT/NDCT images pairs in a specific anatomical region (*e.g.*, the abdomen or the head), researchers devote huge efforts to elaborate powerful reconstructed models with different perspectives, such as edge preservation [6] and texture transfer [7]. Moreover, unpaired CT reconstruction approaches, as more challenging settings, are also developed to tackle the problem of content mismatch between LDCT and NDCT images. To this end, a serial of CycleGAN-based methods [8], [9] are proposed by the means of self-supervised and adversarial schemes. More works about DL-based CT reconstruction can be found in this review [5].

Usually, most existing DL-based CT reconstruction methods implicitly assume that the training CT data (*a.k.a.* source domain D_S) and testing CT data (*a.k.a.* source domain D_T) have a similar noise distribution [6]–[9]. However, the noise distribution between D_S and D_T may be different due to the mismatch of CT scan protocol (*e.g.*, kVp and mAs of the CT scan device) and different anatomical regions (*e.g.*, D_S and D_T from head and abdomen, respectively). This noise distribution shift between D_S and D_T will result in a deterioration of the reconstruction performance, which is recently referred to as **robust CT reconstruction problem** [10]–[12]. Specifically, Lee et al. [10] proposed to model the

noise distribution of target domain via a simple Poisson noise inserting model, such that the pretrained convolutional neural networks (CNNs)-based model on D_S can be transferred to target domain. By leveraging unpaired sinogram data on D_T , Li et al. [11] explicitly model the noise distribution using Gaussian mixture model (GMM) on the target domain to fine-tune the pretrained CNNs-based model on D_S towards target domain.

However, one limitation of abovementioned approaches is that direct explicit noise modeling in the target domain using model-based schemes usually may not have sufficient capacity to represent complex and realistic noise, as discussed by [13], [14], due to the restriction of human knowledge of noise priors (e.g., the assumption of Poisson or Gaussian distribution). This further results in a negative impact of noise transfer from source domain to target domain. Moreover, we can observe that the dynamic changes (as the perturbation) of CT scan protocol (i.e., mAs) in different slices of a patient (see the Figure 1(d)) may cause nonuniform noise distributions in the intra-domain CT images (see the Figure 1(c)), as the tube current modulation is usually on to avoid excessive radiation doses [15]. For this perturbation, existing deterministic neural network (e.g., CNNs)-based CT reconstruction models show insufficient robustness due to their fixed model weights [16]–[18].

To address these problems, we propose to alleviate the noise distribution shifts between source and target domains via implicit noise modeling schemes under a probabilistic framework. Note that we focus more on the robust cross-domain (i.e., D_S and D_T are collected from different anatomical regions) CT reconstruction problem in this paper, as the difference of anatomical region together with scan protocol-related perturbation will lead to more representative and challenging noise distribution shifts (see the Figure 1(c)). Specifically, we introduce a Bayesian-endowed probabilistic framework into the robust cross-domain CT reconstruction problem as illustrated in Figure 2. By doing so, the perturbations of cross-domain samples can be implicitly considered by the distribution of the weights for better robustness. By the virtue of this probabilistic framework, we propose to alleviate the noise distribution shifts between source and target domains in the latent space and image space, respectively. First, we propose to leverage the Bayesian uncertainty of the latent feature endowed by the probabilistic framework to implicitly model the noise distributions of two domains in latent space such that the discrepancy of noise distributions can be reduced. Second, by utilizing the residual information (as a proxy of the noise) between LDCT images and estimated NDCT images in two domains, an adversarial learning manner is imposed to alleviate the discrepancy of noise distribution between source and target domains in the image space.

The contributions of this work can be summarized as following:

- A Bayesian-endowed probabilistic model is introduced into the robust cross-domain CT reconstruction problem for a better robustness.
- A novel Bayesian noise uncertainty alignment (BNUA) method is proposed to conduct implicit noise distribution

modeling and alignment in the latent space.

- The discrepancy of noise distribution shifts between D_S and D_T is reduced by a novel adversarial residual distribution alignment (RDA) scheme in the image space.

II. METHODOLOGY

A. Problem Statement

Here, the source domain with LDCT/NDCT image pairs can be represented as $D_S = \{(\mathbf{x}_1^S, \mathbf{y}_1^S), \dots, (\mathbf{x}_N^S, \mathbf{y}_N^S)\}$, where N denotes that the number of pairs. The target domain has LDCT images only, which can be represented as $D_T = \{\mathbf{x}_1^T, \dots, \mathbf{x}_L^T\}$, where L denotes the number of LDCT images. Suppose that D_S and D_T are available and collected from different anatomical regions with diverse kVp and mAs (as scan protocol-related perturbations), e.g., D_S (D_T) is either the head (abdomen) or the abdomen (head) are different between D_S and D_T . There exists noise distribution shifts between D_S and D_T as shown in Figure 1. By using paired LDCT/NDCT images on D_S and LDCT images on D_T , the objective of robust cross-domain CT reconstruction is to learn a robust model F , which can generalize well on the target domain D_T such that the high-quality reconstructed NDCT image $\hat{\mathbf{y}}^T = F(\mathbf{x}^T)$ on the target domain can be obtained.

B. Robust CT reconstruction under a probabilistic framework

While widely-used deterministic models (e.g., CNNs [19] and self-attention module [20]) have achieved promising performance on the CT reconstruction problem, they show insufficient robustness to input samples that suffer from diverse perturbations (e.g., the dynamic changes of kVs and mAs) even for intra-domain CT construction problem (i.e., both of source and target domains are from the same anatomical region), as discussed by [16], [17]. The underlying reason is that these deterministic models can not incorporate these perturbations as the uncertainty into the prediction directly owing to their fixed model weights. As such, they may be over-confident and produce instability predictions for the perturbation. To address this issue, recent work [17] utilized probabilistic models to render more robust performance for intra-domain CT construction problem. It is no doubt that these scan protocol-related perturbations are more prominent on cross-domain CT reconstruction scenario, as these device parameters (e.g., kVs and mAs) will be modulated dynamically for different anatomical regions [21].

In this paper, we propose to introduce a probabilistic framework into the robust cross-domain CT reconstruction problem. By doing so, the perturbations of cross-domain samples can be implicitly considered by the distribution of the weights as the uncertainty. Specifically, compared with deterministic models, probabilistic models turn to learn a distribution over model weights \mathbf{w} as below,

$$\begin{aligned} \mathbf{w} &= \arg \max_{\mathbf{w}} \log P(\mathbf{w}|D) \\ &= \arg \max_{\mathbf{w}} [\log P(D|\mathbf{w}) + \log P(\mathbf{w})], \end{aligned} \quad (1)$$

where D denotes the training data. The first term is the complexity term, and the second term is a prior distribution of

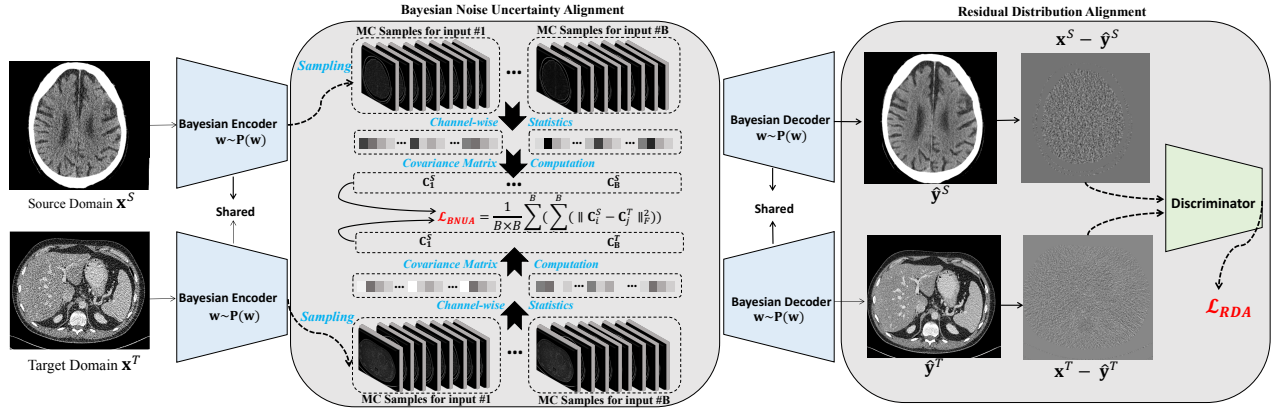


Fig. 2. The overall framework of the proposed method. The CT reconstruction model is disentangled into a BNN-based encoder for the feature extraction and a BNN-based decoder for the content reconstruction from extracted features. By conducting MC sampling, the Bayesian noise uncertainty alignment can be imposed for the alleviation of noise distribution in the latent space. The residual distribution alignment is to align noise distribution of two domains in the image space using the residual information.

the weight that can play a role of implicit regularization for better robustness.

Here, Bayesian neural network (BNN) with variational inference [22], a representative probabilistic model, is introduced to approximate the posterior distribution $P(\mathbf{w}|D)$ of the weight, *i.e.*,

$$\theta^* = \arg \min_{\theta} \text{KL}[q(\mathbf{w}|\theta)||p(\mathbf{w}|D)]. \quad (2)$$

The rationale of variational inference in Eq. 2 is to find the parameters θ of a distribution over the weight in order to minimize the Kullback-Leibler (KL) divergence with its true posterior distribution over the weight. Usually, Eq. 2 can be reformulated as

$$\begin{aligned} \theta^* &= \arg \min_{\theta} \text{KL}[q(\mathbf{w}|\theta)||p(\mathbf{w})] \\ &- \mathbb{E}_{\mathbf{w} \sim p(\mathbf{w}|\theta)} [\log P(D|\mathbf{w})], \end{aligned} \quad (3)$$

where the first term can balance the model complexity with its prior distribution. Moreover, the second term acts an analogous way to the first term in Eq. (1), which aims to fit the training data well as the same as deterministic models (as a reconstruction loss). This objective is so-called evidence lower bound (ELBO) loss. By incorporating the re-parameter trick [23] and stochastic gradient descent method, the variational parameter θ can be solved flexibly.

Different from most existing encoder-decoder-based CT reconstruction models [24], we propose to disentangle a CT reconstruction model into two decoupled probabilistic components (as shown in Figure 2), including a BNN-based encoder (for the feature extraction) and a BNN-based decoder (for the content reconstruction from extracted features), respectively, *i.e.*, $F = E \circ G$. In the next sections, we will describe how to address the noise distribution shifts between D_S and D_T under this probabilistic framework.

C. Bayesian Noise Uncertainty Modeling

For existing cross-domain classification problems, the differences of the image style, texture, and illumination between source and target domains will result in the *domain shift*

problem [25], leading to unfavorable testing performance on target domain. To address this problem, a widely-adopted scheme is to reduce the discrepancy of latent embeddings of two domains by calculating the distance between latent embeddings [26], which can derive robust classification results [27].

Motivated by this strategy, an intuitive idea for robust CT reconstruction is to reduce the noise distribution discrepancy between source and target domains in the latent space, as the *domain shift* of the robust cross-domain CT reconstruction mainly results from the difference of noise distribution. However, the representation of the noise distribution of LDCT images in the latent space is more difficult [28] as the noise appeared in LDCT images is coupled with its content information.

To tackle this issue, we propose to leverage the Bayesian uncertainty to characterize the noise distribution in the latent space, which can in turn to implicitly reflect the noise distribution in the image space. Before introducing our proposed method, the concepts of *Bayesian uncertainty* and Bayesian uncertainty-induced noise encoding [29] derived in the label space need to be reviewed. Specifically, by calculating the variance of different predictions (obtained by multiple Monte Carlo samples) of a same input, Bayesian uncertainty (*i.e.*, the computed variance) can encode the inherent noise on the training data D through the learned distribution of the weight [29]. More importantly, these testing data, which are not consistent with the inherent noise distribution on training data D during inference, will lead to a high uncertainty [29].

Thus, it is reasonable to introduce Bayesian uncertainty from label space into the latent space for latent features (extracted by the BNN-based encoder E) to characterize the noise distribution in the latent space. The rationality of this scheme also can be observed from its probabilistic property, *i.e.*, the posterior distribution $P(\mathbf{w}_E)$ of the weight over the parameterized encoder E is a conditional distribution over $P(\mathbf{w}_E|D)$ given by training data D as Eq. 1. Naturally, Bayesian uncertainty of latent features, *i.e.*, the probabilistic embeddings, $P(\mathbf{z}|\mathbf{x}, \mathbf{w}_E)$, can implicitly encode the noise on

D. Our empirical analysis in the experiment section III-E also shows the rationality of the Bayesian uncertainty.

Furthermore, we can derive that the encoder E trained on the source domain D_S will inherently encode the noise on LDCT images \mathbf{x}^S of the source domain D_S , due to its conditional distribution property. When there exists noise distribution shifts between D_S and D_T , the encoder E trained on source domain D_S will not be generalizable enough to extract the latent features for the LDCT images \mathbf{x}^T on target domain D_T . As a result, it is indeed necessary to reduce the noise distribution discrepancy between source and target domains by minimizing Bayesian uncertainty of the two domains. By doing so, a domain-invariant encoder can be obtained, which means that the latent features \mathbf{z} extracted by this domain-invariant encoder can be fed into the decoder G safely and unbiasedly, leading to better robust cross-domain CT reconstruction results.

Here, how to reduce the noise distribution discrepancy in the latent space via Bayesian uncertainty will be described in detail. Specifically, by feeding two batches of LDCT samples from source and target domains, *i.e.*, $\{\mathbf{x}_i^S\}_{i=1}^B$ and $\{\mathbf{x}_i^T\}_{i=1}^B$ (where $\mathbf{x}_i^{S(T)} \in \mathbb{R}^{W \times H \times 1}$ denotes a LDCT sample with spatial size of $W \times H$ and the channel number of 1. B denotes the number of images in a mini-batch), into the probabilistic encoder E , the output is a probabilistic embedding for each sample, *i.e.*, $P(\mathbf{z}_i^{S(T)} | \mathbf{x}_i^{S(T)}) = P(\mathbf{z}_i^{S(T)} | \mathbf{x}_i^{S(T)}, \mathbf{w}_E)$, where $\mathbf{w}_E \sim P(\mathbf{w}_E)$. The predictive distribution of $P(\mathbf{z}_i^{S(T)} | \mathbf{x}_i^{S(T)})$ can be unbiased approximation using Monte Carlo (MC) estimators with M stochastic sampling operations over the \mathbf{w}_E , *i.e.*,

$$\mathbf{z}_i^{S(T)} = \mathbb{E}[P(\mathbf{z}_i^{S(T)} | \mathbf{x}_i^{S(T)}, \mathbf{w}_E)] = \frac{1}{M} \sum_{j=1}^M E_{\mathbf{w}_E^j}(\mathbf{x}_i^{S(T)}), \quad (4)$$

where $E_{\mathbf{w}_E}(\cdot)$ denotes the parameterized probabilistic encoder, and $\mathbf{z}_i^{S(T)} \in \mathbb{R}^{W' \times H' \times C}$ with C feature channels. By imposing the virtue of probabilistic framework in Eq. 4, we can derive different Bayesian sampling embeddings of a same input \mathbf{x}_i to render Bayesian uncertainty estimation, *i.e.*, $\mathbf{Z}_i^{S(T)} = \{\mathbf{z}_{i,j}^{S(T)}\}_{j=1}^M$, where the subscript j denotes the index of MC sampling and $\mathbf{Z}_i^{S(T)} \in \mathbb{R}^{M \times W' \times H' \times C}$. Here, it is necessary to attain more compact latent feature representation for Bayesian uncertainty estimation, as the information on spatial dimensions $H' \times W'$ are redundant as discussed by [30]. Usually, the channel-wise statistics can reflect more expressive and representative latent features by shrinking the spatial dimensions of latent embeddings, which is observed by previous lectures [31], [32].

By doing so, we utilize the squeeze module in [30] to conduct global information embedding via global average pooling. As such, we can derive a more compact and representative latent features for Bayesian uncertainty estimation in latent space. Specifically, the global average pooling can be imposed for each channel element of each sampling embedding, *i.e.*,

$\mathbf{z}'^{S(T)} \in \mathbb{R}^{W' \times H'}$ as following

$$u^{S(T)} = F_{sq}(\mathbf{z}'^{S(T)}) = \frac{1}{W' \times H'} \sum_{t=1}^{W'} \sum_{q=1}^{H'} z_{t,q}^{S(T)}, \quad (5)$$

where $F_{sq}(\cdot)$ denotes the global average pooling. Finally, the compact latent feature representation can be calculated as $\mathbf{U}_i^{S(T)} = F_{sq}(\mathbf{Z}_i^{S(T)})$, where $\mathbf{U}_i^{S(T)} \in \mathbb{R}^{M \times C}$.

More importantly, we aim to minimize the Bayesian uncertainty discrepancy of obtained latent features $\mathbf{U}_i^{S(T)}$ between source and target domains such that the noise distribution between the two domains can be reduced implicitly. To this end, we propose to leverage the covariance matrix of latent features, as second-order statistics of latent features, to quantify the uncertainty among features. Specifically, we propose to calculate the covariance matrix over different Bayesian sampling embeddings of a same input, *i.e.*, $\mathbf{U}_i^{S(T)}$ as following

$$\begin{aligned} \mathbf{C}_i^S &= \frac{1}{M-1} \sum_{j=1}^M (\mathbf{u}_{i,j}^S - \boldsymbol{\mu}_i^S)^t (\mathbf{u}_{i,j}^S - \boldsymbol{\mu}_i^S), \\ \mathbf{C}_i^T &= \frac{1}{M-1} \sum_{j=1}^M (\mathbf{u}_{i,j}^T - \boldsymbol{\mu}_i^T)^t (\mathbf{u}_{i,j}^T - \boldsymbol{\mu}_i^T), \end{aligned} \quad (6)$$

where $\boldsymbol{\mu}_i^S$ and $\boldsymbol{\mu}_i^T$ denote the mean of the \mathbf{U}_i^S and \mathbf{U}_i^T , respectively. $\mathbf{u}_{i,j}^S$ and $\mathbf{u}_{i,j}^T$ represent the j -th row of the \mathbf{U}_i^S and \mathbf{U}_i^T . The size of \mathbf{C}_i^S and \mathbf{C}_i^T is $C \times C$.

Note that the calculation in Eq. 6 is different from existing covariance matrix alignment of latent features (*e.g.*, CORAL [33]) in cross-domain classification problems, as the covariance matrix in Eq. 6 is derived from the different Bayesian sampling embeddings of a same sample rather than different samples in the source (or target) domain, which means that our proposed method can ignore the interference of content information (as the content information are same for different sampling embeddings of a same input), and then focus more on the uncertainty estimate of latent features.

Finally, the Bayesian uncertainty discrepancy as a \mathcal{L}_{BNUA} objective in a batch of samples between source and target domains can be minimized as below,

$$\mathcal{L}_{BNUA} = \frac{1}{B \times B} \sum_{i=1}^B \sum_{j=1}^B \|\mathbf{C}_i^S - \mathbf{C}_j^T\|_F^2, \quad (7)$$

where $\|\cdot\|_F$ denotes the Frobenius norm. In this paper, the objective \mathcal{L}_{BNUA} is called as **Bayesian Noise Uncertainty Alignment** (BNUA) loss due to its Bayesian property and implicit noise modeling via uncertainty estimation. Our proposed Bayesian noise uncertainty alignment has several advantages as following. First, it is an unsupervised manner as the computation in Eq. 7 does not refer to any NDCT images on the target domain D_T . Second, it is a **parameter-free** manner, as there are no additional parameters in the BNUA module need to be learned. Instead, existing noise modeling methods (*e.g.*, GMM) need to solve extra parameters (*e.g.*, mixing coefficients via EM algorithm). Third, compared with existing explicit noise distribution representation methods on image domain, the proposed implicit noise modeling in latent space via Bayesian uncertainty may be more powerful.

D. Residual Distribution Alignment via Adversarial Training

In the previous section, we figure out how to conduct the implicit noise distribution alignment via minimizing Bayesian uncertainty discrepancy in the latent space. Then, the encoder may be regularized to render the domain-invariant feature embeddings between source and target domains. However, it is also important to reduce the discrepancy of noise distribution between source and target domains in the image space, as this discrepancy may affect the quality of reconstructed CT images (*i.e.*, estimated NDCT images) directly.

How to characterize the noise distribution in the image space is an urgent issue. Here, we can first recall the widely-used LDCT image degraded model, *i.e.*, $\mathbf{x} = \mathbf{y} + \mathbf{n}$, where \mathbf{x} , \mathbf{y} and \mathbf{n} denote the LDCT image, the NDCT image and the noise in the image space, respectively. According to the degraded model, we can derive a simple yet effective noise estimation method through the residual information (as a proxy of the noise), *i.e.*, $\hat{\mathbf{n}} = \mathbf{x} - \hat{\mathbf{y}}$, where $\hat{\mathbf{y}} = F(\mathbf{x})$ denotes the estimated NDCT images by the reconstruction model. By recalling the residual information, the noises on source and target domains, *i.e.*, $\hat{\mathbf{n}}^S$ and $\hat{\mathbf{n}}^T$, can be approximated through their corresponding residual information. Note that the supervised information on the source domain (*e.g.*, \mathbf{x}^S and \mathbf{y}^S) can guarantee the relative usability of estimated noises on the source and target domains. Moreover, quite a few cross-domain classification methods also leverage the predictions on the target domain (during training) as a complementary information (*a.k.a.* pseudo label) to guide a promising cross-domain performance [34], [35]. Similarly, the estimated noise on target domain $\hat{\mathbf{n}}^T$ benefits from estimated (pseudo) NDCT images $\hat{\mathbf{y}}^T$ on target domain during training, *i.e.*, $\hat{\mathbf{n}}^T = \mathbf{x}^T - \hat{\mathbf{y}}^T$. One can observe that this scheme is also decoupled with the content information existed on the LDCT image as much as possible, as the residual information is derived from a same LDCT image \mathbf{x} .

According to obtained estimated noises on source and target domains, reducing noise distribution discrepancy between the two domains may be feasible in the image space. It should be noted that the distributions of NDCT images on the source and target domain may be different depending on their specific anatomical regions, which means $P(\mathbf{y}^T|\mathbf{x}^T) \neq P(\mathbf{y}^S|\mathbf{x}^S)$. Instead, forcing the noise distribution of source domain $P(\mathbf{n}^S)$ to converge towards the noise distribution of target domain $P(\mathbf{n}^T)$ becomes more reasonable. To this end, we utilize an adversarial learning manner to reduce the noise distribution discrepancy between source and target domains (namely residual distribution alignment (RDA)).

Specifically, a parameterized discriminator D can be utilized to distinguish whether the estimated noise $\hat{\mathbf{n}}^S$ on source domain is similar with the estimated noise $\hat{\mathbf{n}}^T$ on target domain. The significant discrepancy of noise distribution between the two domains will induce a high discriminator loss, which would push the reconstruction model F to reduce the noise distribution gap. Here, we adopt the LSGAN [36]-based adversarial learning process due to its more stable convergence,

which can be formulated as following,

$$\begin{aligned} \min_{\theta_D} \mathcal{L}(D) &= \mathbb{E}_{\mathbf{x}^T \sim P(\mathbf{x}^T)} [D[\mathbf{x}^T - G(E(\mathbf{x}^T))] - 1] \\ &+ \mathbb{E}_{\mathbf{x}^S \sim P(\mathbf{x}^S)} [D[\mathbf{x}^S - G(E(\mathbf{x}^S))] - 0], \\ \min_{\mathbf{w}_E, \mathbf{w}_G} \mathcal{L}(E, G) &= \mathbb{E}_{\mathbf{x}^S \sim P(\mathbf{x}^S)} [D[\mathbf{x}^S - G(E(\mathbf{x}^S))] - 1]. \end{aligned} \quad (8)$$

One can observe from Eq 8 that the noise distribution discrepancy between source and target domains will be reduced gradually though optimizing two adversarial losses for the discriminator D and the reconstruction model $F = E \circ G$. Moreover, the reconstruction loss between the estimated NDCT images $\hat{\mathbf{y}}^S$ and corresponding ground-truth NDCT images \mathbf{y}^S on the source domain would avoid an excessive noise distribution transfer from source domain to target one. By balancing the adversarial loss and reconstruction loss, our proposed method can minimize the noise distribution discrepancy between domains to obtain a transferable noise distribution. By doing so, a robust cross-domain CT reconstruction model is prone to be learned.

E. Model Training and Overall Framework

Our proposed robust cross-domain CT reconstruction framework consists of three modules, including a probabilistic encoder, a probabilistic decoder, and a discriminator. For the probabilistic encoder and decoder, we follow the structure of the popular CT reconstruction backbone, *i.e.*, a widely-adopted CPCE model [24]. To balance the computational consumption with the sufficient probabilistic property, we follow [37] to only replace the last layer of the encoder and the decoder with its Bayesian neural network version. Specifically, the last layer of the encoder is a Bayesian-based CNN layer with 32 channels and 3×3 kernel size. The last layer of the decoder is a Bayesian-based deconvolutional layer with 1 channel and 3×3 kernel size. The structure of the discriminator in the RDA module is the same as that of CycleGAN [38]. The overall objective of our proposed framework consists of three components, including a ELBO loss, a Bayesian noise uncertainty alignment loss, and a distributional alignment loss. Here, the reconstruction term of ELBO loss is guided from both image space (*i.e.*, the mean absolute error) and feature space (*i.e.*, the perceptual loss [39] $PL(\cdot, \cdot)$). The overall objective can be computed as following,

$$\begin{aligned} \mathcal{L} &= \sum_i [\|\mathbf{y}_i^S - \hat{\mathbf{y}}_i^S\|_1 + PL(\mathbf{y}_i^S, \hat{\mathbf{y}}_i^S)] + \text{KL}[q_\theta(Q_\phi) \| p(Q_\phi)] \\ &+ \text{KL}[q_\theta(C_\omega) \| p(C_\omega)] + \beta_1 \mathcal{L}_{BNUA} + \beta_2 \mathcal{L}_{RDA}, \end{aligned} \quad (9)$$

where the variance of log likelihood is set to 1 for simplification computed by the ground-truth \mathbf{y}_i and its estimation $\hat{\mathbf{y}}_i$. The third and fourth terms aim to learn a variational distribution $q_\theta(\cdot)$ to approximate the Bayesian posterior distribution on the weights, while minimizing the KL divergence with its prior distribution $p(\cdot)$. β_1 and β_2 control the influence of the BNUA module and RDA module, respectively.

TABLE I
THE DETAILS OF USED DATASETS FOR THE VALIDATION OF THE ROBUST
CROSS-DOMAIN CT RECONSTRUCTION TASK.

<i>Dataset</i>	<i>Domain A</i>	<i>Domain B</i>
Scanning parts	Abdomen	Head
kVs	100	120
mAs	Dynamic	Dynamic
Resolution	512 × 512	512 × 512
Training Images	3952 (7 patients)	1476 (49 patients)
Validation Images	850 (1 patient)	35 (1 patient)
Testing Images	1108 (2 patients)	131 (4 patients)

III. EXPERIMENTS AND ANALYSES

A. Datasets and Training Protocol

In this paper, the performance of the proposed robust cross-domain CT reconstruction is validated on public clinical dataset, i.e., the Low Dose CT Image and Projection Data (LDCT-and-Projection-data)¹, which is released by Mayo Clinic, where **abdomen** (namely *Domain A*) and **head** (namely *Domain B*) CT scans are utilized as the cross-domain CT reconstruction task. In the LDCT-and-Projection-data dataset, both normal-dose and simulated low (quarter)-dose CT image are reconstructed using commercial CT system with a filtered back projection method. There are 10 patients’ abdomen CT scans, where 7 patients for training, 1 patient for validation, and 2 patient for testing. Moreover, there are 54 patients’ head CT scans, where 49 patients for training, 1 patient for validation, and 4 patient for testing. As shown in Figure 3, the significant noise distribution shifts between the abdomen and head scans can be observed (see the third column of Figure 3 and corresponding probability density function (PDF). As a result, the robust cross-domain CT reconstruction is a challenging and meaningful task. More details about the used datasets can be found in Table I. For data preprocessing, all CT scans are normalized into $0 \sim 1$ with anatomical-specific window widths (head: 90 and abdomen: 400) and window levels (head: 35 and abdomen: 40). Each of CT scans is randomly split into 8 patches with the size of 64 for training.

Here, $A \rightarrow B$ denotes a robust cross-domain CT reconstruction task, where the abdomen and head CT images as the source and target domains, respectively, and vice versa. Thus, there are two robust cross-domain CT reconstruction tasks.

B. Implement Details

The proposed robust cross-domain CT reconstruction model is implemented by Pytorch and BayesianTorch². We adopt mean-field variational inference (MFVI) [40] for the analytical approximation of the Bayesian layer, where the parameters are characterized by fully factorized Gaussian distribution endowed by variational parameters μ and σ , i.e. $q_{\theta}(w) := \mathcal{N}(w|\mu, \sigma)$. By using BayesianTorch, deterministic neural networks can be transformed easily into their Bayesian versions. For the parameter settings of Bayesian weight priors, empirical Bayes using DNN (MOPED) [41] method is used, where the initial perturbation factor δ for the weight to 0.1. The number of MC sampling during training is set to 10 empirically.

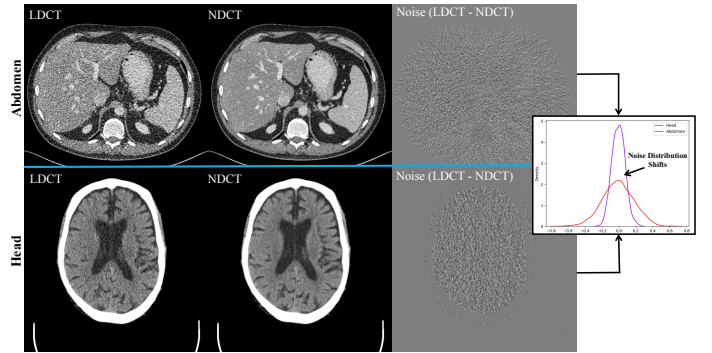


Fig. 3. Example samples of the used abdomen and head datasets. The noise map of each LDCT image (in the third column) is obtained by the subtraction between the LDCT image and corresponding NDCT image. The display windows for the head scan and the abdomen scan are $[-10,80]$ and $[-160,240]$, respectively.

The parameters of the overall model are updated by Adam optimizer with the learning rate as 1×10^{-4} . The number of the mini-batch is set to 32. For each robust cross-domain task, the training set consists of the paired LDCT/NDCT data in the training set of the source domain and the LDCT data in the training set of the target domain. The important hyperparameters of our proposed method, including β_1 and β_2 , are selected on the validation set of the source domain. Specifically, β_1 and β_2 are set to 10 and 0.001 for two robust cross-domain tasks, respectively. Moreover, the robust cross-domain performance of the model is evaluated on the testing set of the target domain.

C. Baseline Methods and Evaluation Metrics

In this paper, we compare our proposed method with some representative CT reconstruction approaches, including Block-matching and 3D filtering (BM3D) method [42], optimized non-local means (ONLM) method for CT reconstruction [43], Noiser2noise [44], CycleGAN [38], unsupervised domain adaptation method for LDCT denoising (UDA-LDCT) [10], semantic information alignment-based cross-domain LDCT denoising (SIA-LDCT) method [12]. Note that BM3D and ONLM are traditional model-based LDCT image reconstruction method. Noiser2noise only refers to the LDCT images on target domain to conduct unsupervised image denoising. By utilizing the LDCT images on target domain and the NDCT images on source domain, CycleGAN can learn a transferable style from target domain to source domain [38]. Compared with our proposed method, UDA-LDCT and SIA-LDCT aim to address the noise distribution shifts between source and target domains with a similar anatomical region. Note that we also introduce a MFVI-based Bayesian neural network (MF-BNN) [45] as a baseline model, which is only trained by paired source domain data. Except for imposing additional \mathcal{L}_{BNUA} and \mathcal{L}_{RDA} modules, the network structure of our proposed method is equal to that of the MF-BNN. The hyperparameters of baseline methods are tuned in a wide range on the validation set of the source domain.

To comprehensively evaluate the performance of different models, we introduce two kinds of evaluation approaches, in-

¹<https://wiki.cancerimagingarchive.net/pages/>

²<https://github.com/IntelLabs/bayesian-torch>

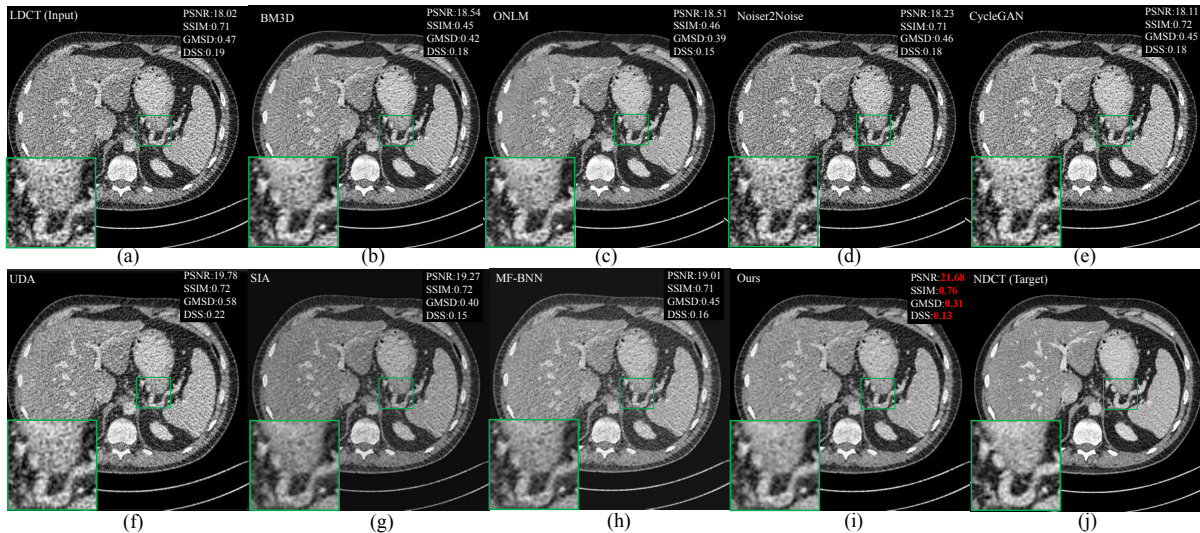


Fig. 4. The visual comparison among different baseline methods for $\mathcal{A} \rightarrow \mathcal{B}$ robust cross-domain CT reconstruction task. The green box on the left bottom of each image is the zoomed-in view of the selected ROI. The quantitative results of each image are listed in the top right corner. The display window is [-160,240].

TABLE II

THE EXPERIMENTAL RESULTS ON THE ROBUST CROSS-DOMAIN CT RECONSTRUCTION TASK FROM $\mathcal{A} \rightarrow \mathcal{B}$, *i.e.*, THE HEAD CT IMAGES AS THE SOURCE DOMAIN AND THE ABDOMEN CT IMAGES AS THE TARGET DOMAIN. THE AVERAGE VALUE AND STANDARD DEVIATION ARE REPORTED BY RUNNING EACH METHOD WITH FIVE TIMES. FOR PSNR AND SSIM, THE HIGHER, THE BETTER. FOR GMSD AND DSS, THE LOWER, THE BETTER.

Method	PSNR \uparrow	SSIM \uparrow	GMSD \downarrow	DSS \downarrow
MF-BNN	19.2601 \pm 0.1769	0.4892 \pm 0.0121	0.1789 \pm 0.0012	0.3556 \pm 0.0011
BM3D	20.2815 \pm 0.1976	0.5824 \pm 0.0201	0.2001 \pm 0.0101	0.4618 \pm 0.0009
ONLM	20.0401 \pm 0.1622	0.5741 \pm 0.0321	0.1677 \pm 0.0154	0.3101 \pm 0.0003
Noiser2Noise	19.4195 \pm 0.1893	0.5412 \pm 0.0211	0.1775 \pm 0.0178	0.3795 \pm 0.0011
CycleGAN	19.3777 \pm 0.2001	0.5436 \pm 0.0134	0.1887 \pm 0.0221	0.3863 \pm 0.0010
UDA-LDCT	19.9717 \pm 0.1799	0.5011 \pm 0.0982	0.1499 \pm 0.0120	0.3316 \pm 0.0004
SIA-LDCT	20.2965 \pm 0.1828	0.5894 \pm 0.0114	0.1693 \pm 0.0203	0.3312 \pm 0.0027
Ours	22.7201\pm0.1782	0.6137\pm0.0213	0.1269\pm0.0104	0.2519\pm0.0003

cluding image-based evaluation metrics and perception-based evaluation metrics. The former includes the peak signal-to-noise ratio (PSNR) and the structural similarity index measure (SSIM) [46]. The latter includes the gradient magnitude similarity deviation (GMSD) [47] and discrete cosine transform-based sub-bands similarity index (DSS) [48], which both derive from human visual system (as an efficient perceptual image quality tool).

D. Experimental Results

Source: Head, Target: Abdomen. First, we utilize the head scans as the source domain and the abdomen scans as the target domain. We can analyze from Figure 3 that the noise distribution shifts between source and target domains mainly result from the mismatch of the noise level (*e.g.*, the variance of the noise distribution). Specifically, the noise level of the head scans is roughly lower than that of the abdomen scans. As a result, the model trained on head scans may not be

powerful to remove the noise from the abdomen scans, which is a challenging domain gap.

The quantitative results of different baseline methods are reported in the Table II. We have some observations as follows: First, our proposed method outperforms all baseline methods with a clear margin. Second, UDA-LDCT, SIA-LDCT and our proposed method roughly achieve better performance (especially for the PSNR, GMSD and DSS) than Noiser2noiser and CycleGAN, which is reasonable as these cross-domain CT reconstruction methods can leverage extra supervised information from the source domain compared with unsupervised/unpaired schemes. However, compared with UDA-LDCT and SIA-LDCT, our proposed method not only can alleviate the noise distribution shifts between the source and target domains via the noise distribution alignment in the latent and image space, but also can avoid the negatively transferable effect resulting from the difference of anatomical structure. Third, although BM3D and ONLM can obtain acceptable performance in terms of PSNR and SSIM, the perceptual quantitative results (such as GMSD and DSS) are significantly worse than what our proposed method achieves.

The visual comparison among different baseline approaches is shown in Figure 4. We can observe from the zoomed-in view that our proposed method not only can suppress the noise well (please see the region of low resistance in the top right corner), but also can have a more natural texture to the NDCT images (compared with BM3D, ONLM, Noiser2noise, and CycleGAN). Moreover, our proposed method has a good contrast compared with SIA-LDCT and MF-BNN.

Source: Abdomen, Target: Head. The second robust cross-domain CT reconstruction task is from abdomen scans (as the source domain) to head scans (as the target domain). The quantitative results of different baseline methods are reported in the Table III. some observations can be noticed as following: First, except for the PSNR, our proposed method outperforms the best performance compared with other baseline methods,

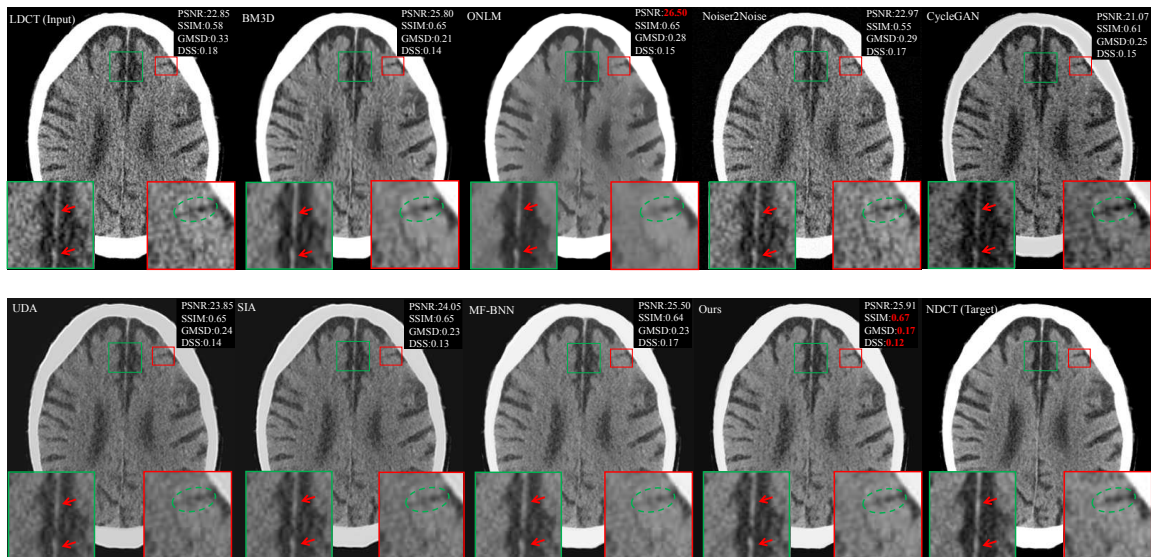


Fig. 5. The visual comparison among different baseline methods for $\mathcal{B} \rightarrow \mathcal{A}$ robust cross-domain CT reconstruction task. The green and red boxes on the left and right bottom of each image are the zoomed-in view of the selected ROIs. The quantitative results of each image are listed in the top right corner. The display window is $[-10,80]$.

TABLE III

THE EXPERIMENTAL RESULTS ON THE ROBUST CROSS-DOMAIN CT RECONSTRUCTION TASK FROM $\mathcal{B} \rightarrow \mathcal{A}$, *i.e.*, THE ABDOMEN CT IMAGES AS THE SOURCE DOMAIN AND THE HEAD CT IMAGES AS THE TARGET DOMAIN. THE AVERAGE VALUE AND STANDARD DEVIATION ARE REPORTED BY RUNNING EACH METHOD WITH FIVE TIMES. FOR PSNR AND SSIM, THE HIGHER, THE BETTER. FOR GMSD AND DSS, THE LOWER, THE BETTER.

Method	PSNR \uparrow	SSIM \uparrow	GMSD \downarrow	DSS \downarrow
MF-BNN	24.3351 \pm 0.1336	0.6386 \pm 0.0075	0.1439 \pm 0.0026	0.2349 \pm 0.0041
BM3D	25.7475 \pm 0.1801	0.6525 \pm 0.0112	0.1534 \pm 0.0092	0.3530 \pm 0.0009
ONLM	26.6574 \pm 0.3231	0.6466 \pm 0.0282	0.1501 \pm 0.1231	0.3090 \pm 0.0213
Noiser2Noise	23.8407 \pm 0.1589	0.5792 \pm 0.0313	0.1628 \pm 0.0091	0.3132 \pm 0.0233
CycleGAN	23.7163 \pm 0.4285	0.6160 \pm 0.0382	0.1537 \pm 0.0093	0.3180 \pm 0.0224
SIA-LDCT	23.0560 \pm 0.1961	0.6403 \pm 0.0218	0.1375 \pm 0.0031	0.2738 \pm 0.0103
UDA-LDCT	22.4791 \pm 0.3118	0.6192 \pm 0.0435	0.1773 \pm 0.0022	0.3421 \pm 0.0226
Ours	25.4989 \pm 0.1478	0.6642 \pm 0.0345	0.1253 \pm 0.0017	0.1950 \pm 0.0196

in terms of SSIM, GMSD, and DSS. Instead, although ONLM and BM3D achieves the best and the second-best performances for PSNR and SSIM, they do not have competitive perceptual scores (such as GMSD and DSS) compared with our proposed method. This phenomenon can be reflected by the visualized comparison in Figure 5. Specifically, it seems that BM3D and ONLM have better capacity for noise removal compared with our proposed method (see the zoomed-in green box). However, we can observe that 1) BM3D suffers from the over-smooth problem (see the green circle of the zoomed-in red box), leading to the unnatural texture compared with NDCT image. 2) ONLM losses the tiny structure due to the excessive noise removal (see the green circle of the zoomed-in red box). Instead, our proposed method achieves better noise suppression compared with other deep learning-based method (see the red arrow of the zoomed-in green box). Moreover, a more natural texture and good structure retaining can be realized compared with traditional model-based approaches.

TABLE IV

ABLATION STUDY ON DIFFERENT COMPONENTS ON $A \rightarrow B$ ROBUST CROSS-DOMAIN CT RECONSTRUCTION TASK.

Setting	Deterministic	Bayesian	BNUA	RDA	PSNR \uparrow	SSIM \uparrow	GMSD \downarrow	DSS \downarrow
1	✓				18.9901 \pm 0.4311	0.4501 \pm 0.0202	0.1923 \pm 0.0101	0.3723 \pm 0.0013
2		✓			19.2601 \pm 0.2112	0.4892 \pm 0.0121	0.1789 \pm 0.0012	0.3556 \pm 0.0011
3		✓	✓		21.7201 \pm 0.1988	0.6097 \pm 0.0210	0.1409 \pm 0.0211	0.2909 \pm 0.0011
4		✓	✓	✓	21.1312 \pm 0.1622	0.6001 \pm 0.0112	0.1298 \pm 0.0201	0.2592 \pm 0.0014
5		✓	✓	✓	22.7201 \pm 0.2342	0.6137 \pm 0.0213	0.1269 \pm 0.0104	0.2519 \pm 0.0003

E. Further analysis

In this section, we first explore the effectiveness of each component in our proposed framework on robust cross-domain CT reconstruction task.

Deterministic Framework v.s. Probabilistic Framework. To validate the effectiveness of the probabilistic framework, we compare the deterministic CPCE model with our adopted Bayesian version. The quantitative results on the $A \rightarrow B$ task are reported in Table IV. From the first and the second rows of Table IV, we can observe the probabilistic framework outperforms the deterministic framework, especially for the SSIM score, which is reasonable as the probabilistic property of the weights in Bayesian network can act an implicit regularization for better robustness.

Effectiveness of Bayesian Noise Uncertainty Alignment (BNUA). BNUA module aims to alleviate the noise distribution discrepancy between the source and target domains in the latent space. Here, we can notice from the third row of Figure IV that the PSNR and SSIM scores are improved significantly via equipping the \mathcal{L}_{BNUA} , compared with Bayesian neural network (in the second row, as a baseline). Furthermore, by testing on the validation set, we compute the Bayesian uncertainty discrepancy between source and target domains (as described in Eq. 7) of different models (including the baseline model and the baseline + \mathcal{L}_{BNUA} model). The quantitative results can be found in Figure 7. As we can see, the baseline

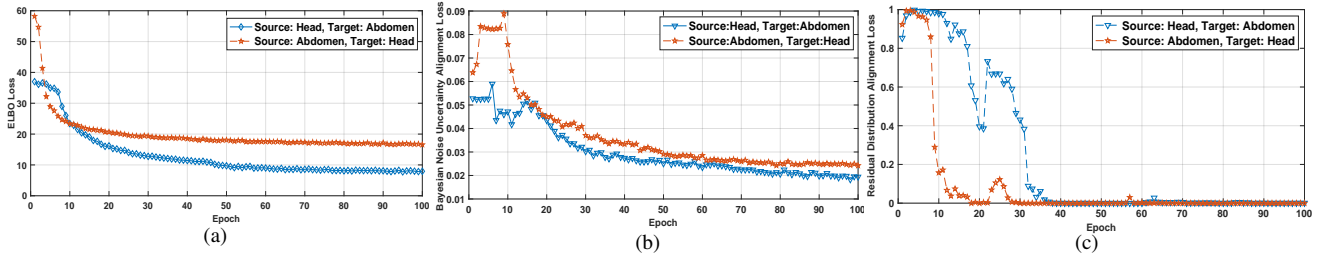


Fig. 6. The convergence curves of different losses during the training.

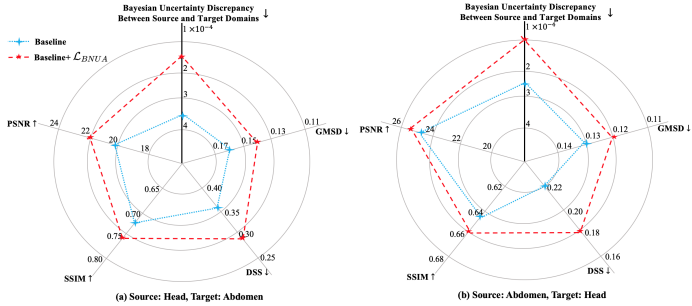


Fig. 7. The relationship between Bayesian uncertainty discrepancy (between source and target domains) and quantitative results on validation set. The Bayesian uncertainty discrepancy can be computed using Eq. 7. The average value is reported by running each model with 10 times. Please zoom in for better view.

model, who does not adopt any noise distribution alignment strategy, suffers from a bigger Bayesian uncertainty discrepancy for both two tasks (see the blue star on the bold black line), which reflects the Bayesian uncertainty discrepancy can implicitly represent the noise distribution gap of two domains in the latent space. Instead, by imposing the \mathcal{L}_{BNUA} , the model has a smaller Bayesian uncertainty discrepancy (see the red pentagram on the bold black line), which also contributes to better quantitative results.

Effectiveness of Residual Distribution Alignment (RDA). RDA aims to reduce noise distribution discrepancy between source and target domains in the image space through the residual information (as the proxy of noise). By introducing an adversarial manner, we can observe from the fourth row of the Figure IV that the quantitative results (especially for the GMSD and DSS) are improved with a clear margin compared with the baseline method. In the Figure 8, we plot the probability density functions (PDFs) of selected ROIs in the region of low resistance (which can reflect the noise distribution as much as possible). We can notice that the baseline method and corresponding RDA version can achieve an acceptable transfer from LDCT image to reconstructed image. However, the RDA version (see the red curve) is closer to the NDCT image (see the purple curve), which is reasonable as the discriminator in the RDA scheme can force the model to reduce the noise distribution (using the residual information as a proxy) discrepancy between source and target domains such that a better robust cross-domain CT reconstruction performance can be realized.

Empirical Convergence Analysis of Different Losses. Our

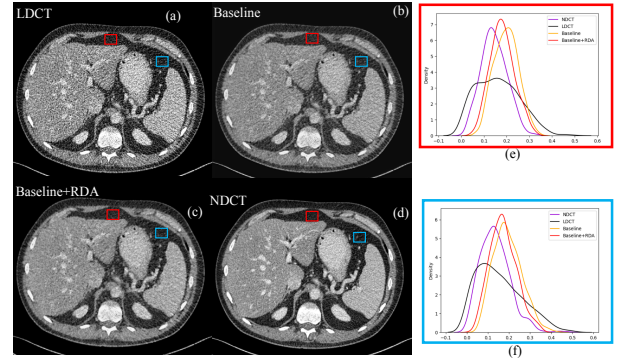


Fig. 8. The probability density functions (PDFs) of selected ROIs in the region of low resistance.

proposed method includes the ELBO loss, BNUA loss and RDA loss. Here, we conduct an empirical convergence analysis of different losses. As shown in Figure 6, we can observe that the ELBO loss and RDA loss have a faster convergence speed than the BNUA loss during training.

IV. CONCLUSION

In this paper, we address the problem of robust computed tomography (CT) reconstruction issue under a cross-domain scenario. A Bayesian-endowed probabilistic framework is introduced into a robust cross-domain CT reconstruction task. Under this probabilistic framework, we propose to alleviate the noise distribution shifts between source and target domains via implicit noise modeling schemes in the latent space and image space. Specifically, A novel Bayesian noise uncertainty alignment (BNUA) method is proposed to conduct implicit noise distribution modeling and alignment in the latent space. Moreover, the discrepancy of noise distribution shifts between D_S and D_T is reduced by a novel adversarial residual distribution alignment (RDA) scheme in the image space. Extensive experiments show that our proposed method can achieve a better performance of robust cross-domain CT reconstruction than existing methods.

REFERENCES

- [1] Z. Yin, K. Xia, S. Wang, Z. He, J. Zhang, and B. Zu, "Unpaired low-dose ct denoising via an improved cycle-consistent adversarial network with attention ensemble," *The Visual Computer*, pp. 1–22, 2022. 1
- [2] L. Yang, Z. Li, R. Ge, J. Zhao, H. Si, and D. Zhang, "Low-dose ct denoising via sinogram inner-structure transformer," *IEEE Transactions on Medical Imaging*, 2022. 1

- [3] C. Niu, M. Li, X. Guo, and G. Wang, "Self-supervised dual-domain network for low-dose ct denoising," in *Developments in X-Ray Tomography XIV*, vol. 12242. SPIE, 2022. I
- [4] A. Bonney, R. Malouf, C. Marchal, D. Manners, K. M. Fong, H. M. Marshall, L. B. Irving, and R. Manser, "Impact of low-dose computed tomography (ldct) screening on lung cancer-related mortality," *Cochrane Database of Systematic Reviews*, no. 8, 2022. I
- [5] G. Wang, J. C. Ye, and B. De Man, "Deep learning for tomographic image reconstruction," *Nature Machine Intelligence*, vol. 2, no. 12, pp. 737–748, 2020. I
- [6] Z. Guo, F. Zhou, Y. Chen, and J. Yuan, "A low-dose ct image denoising method combining multistage network and edge protection," *Tehnički vjesnik*, vol. 29, no. 3, pp. 1059–1067, 2022. I, I
- [7] H. Wang, X. Zhao, W. Liu, L. C. Li, J. Ma, and L. Guo, "Texture-aware dual domain mapping model for low-dose ct reconstruction," *Medical Physics*, 2022. I, I
- [8] J. Gu and J. C. Ye, "Adain-based tunable cyclegan for efficient unsupervised low-dose ct denoising," *IEEE Transactions on Computational Imaging*, vol. 7, pp. 73–85, 2021. I, I
- [9] L. Shi-min, L. Yang-chuan, Z. Ye-chen, W. Yan-ling, and G. Xin, "An improved low-dose ct image enhancement network based on cyclegan," *Journal of Graphics*, vol. 43, no. 4, p. 570, 2022. I, I
- [10] J.-Y. Lee, W. Kim, Y. Lee, J.-Y. Lee, E. Ko, and J.-H. Choi, "Unsupervised domain adaptation for low-dose computed tomography denoising," *IEEE Access*, 2022. I, III-C
- [11] D. Li, Z. Bian, S. Li, J. He, D. Zeng, and J. Ma, "Noise characteristics modeled unsupervised network for robust ct image reconstruction," *IEEE Transactions on Medical Imaging*, 2022. I
- [12] J. Huang, K. Chen, J. Sun, X. Pu, and Y. Ren, "Cross domain low-dose ct image denoising with semantic information alignment," in *2022 IEEE ICIP*. IEEE, 2022, pp. 4228–4232. I, III-C
- [13] H. Lu, H. Han, and S. K. Zhou, "Dual-gan: Joint bvp and noise modeling for remote physiological measurement," in *CVPR*, 2021, pp. 12404–12413. I
- [14] J. Chen, J. Chen, H. Chao, and M. Yang, "Image blind denoising with generative adversarial network based noise modeling," in *CVPR*, 2018, pp. 3155–3164. I
- [15] M. K. Kalra, M. M. Maher, T. L. Toth, B. Schmidt, B. L. Westerman, H. T. Morgan, and S. Saini, "Techniques and applications of automatic tube current modulation for ct," *Radiology*, vol. 233, no. 3, pp. 649–657, 2004. I
- [16] V. Antun, F. Renna, C. Poon, B. Adcock, and A. C. Hansen, "On instabilities of deep learning in image reconstruction and the potential costs of ai," *Proceedings of the National Academy of Sciences*, vol. 117, no. 48, pp. 30088–30095, 2020. I, II-B
- [17] M. Tölle, M.-H. Laves, and A. Schlaefer, "A mean-field variational inference approach to deep image prior for inverse problems in medical imaging," in *Medical Imaging with Deep Learning*. PMLR, 2021, pp. 745–760. I, II-B
- [18] Z. Eaton-Rosen, F. Bragman, S. Bisdas, S. Ourselin, and M. J. Cardoso, "Towards safe deep learning: accurately quantifying biomarker uncertainty in neural network predictions," in *MICCAI*. Springer, 2018, pp. 691–699. I
- [19] H. Shan, A. Padole, F. Homayounieh, U. Kruger, R. D. Khera, C. Nitiwarangkul, M. K. Kalra, and G. Wang, "Competitive performance of a modularized deep neural network compared to commercial algorithms for low-dose ct image reconstruction," *Nature Machine Intelligence*, vol. 1, no. 6, p. 269, 2019. II-B
- [20] M. Li, W. Hsu, X. Xie, J. Cong, and W. Gao, "Sacnn: Self-attention convolutional neural network for low-dose ct denoising with self-supervised perceptual loss network," *IEEE transactions on medical imaging*, vol. 39, no. 7, pp. 2289–2301, 2020. II-B
- [21] Y. Inoue, K. Nagahara, H. Kudo, and H. Itoh, "Ct dose modulation using automatic exposure control in whole-body pet/ct: effects of scout imaging direction and arm positioning," *American Journal of Nuclear Medicine and Molecular Imaging*, vol. 8, no. 2, p. 143, 2018. II-B
- [22] M. D. Hoffman, D. M. Blei, C. Wang, and J. Paisley, "Stochastic variational inference," *Journal of Machine Learning Research*, 2013. II-B
- [23] R. Tian, Y. Mao, and R. Zhang, "Learning vae-lda models with rounded reparameterization trick," in *EMNLP*, 2020, pp. 1315–1325. II-B
- [24] H. Shan, Y. Zhang, Q. Yang, U. Kruger, M. K. Kalra, L. Sun, W. Cong, and G. Wang, "3-d convolutional encoder-decoder network for low-dose ct via transfer learning from a 2-d trained network," *IEEE transactions on medical imaging*, vol. 37, no. 6, pp. 1522–1534, 2018. II-B, II-E
- [25] H. Li, S. J. Pan, S. Wang, and A. C. Kot, "Domain generalization with adversarial feature learning," in *Proceedings of the IEEE conference on computer vision and pattern recognition*, 2018, pp. 5400–5409. II-C
- [26] M. Wang and W. Deng, "Deep visual domain adaptation: A survey," *Neurocomputing*, vol. 312, pp. 135–153, 2018. II-C
- [27] W. M. Kouw and M. Loog, "A review of domain adaptation without target labels," *IEEE transactions on pattern analysis and machine intelligence*, vol. 43, no. 3, pp. 766–785, 2019. II-C
- [28] K. Chen, J. Huang, J. Sun, Y. Ren, and X. Pu, "Task-driven deep learning for ldct image denoising," in *The Fourth International Symposium on Image Computing and Digital Medicine*, 2020, pp. 35–39. II-C
- [29] D. Hafner, D. Tran, A. Irpan, T. Lillicrap, and J. Davidson, "Reliable uncertainty estimates in deep neural networks using noise contrastive priors," *stat*, vol. 1050, p. 24, 2018. II-C, II-C
- [30] J. Hu, L. Shen, and G. Sun, "Squeeze-and-excitation networks," in *CVPR*, 2018, pp. 7132–7141. II-C, II-C
- [31] J. Yang, K. Yu, Y. Gong, and T. Huang, "Linear spatial pyramid matching using sparse coding for image classification," in *CVPR*. IEEE, 2009, pp. 1794–1801. II-C
- [32] L. Shen, G. Sun, Q. Huang, S. Wang, Z. Lin, and E. Wu, "Multi-level discriminative dictionary learning with application to large scale image classification," *IEEE Transactions on Image Processing*, vol. 24, no. 10, pp. 3109–3123, 2015. II-C
- [33] B. Sun, J. Feng, and K. Saenko, "Return of frustratingly easy domain adaptation," in *Proceedings of the AAAI Conference on Artificial Intelligence*, vol. 30, no. 1, 2016. II-C
- [34] Q. Wang and T. Breckon, "Unsupervised domain adaptation via structured prediction based selective pseudo-labeling," in *AAAI*, vol. 34, no. 04, 2020, pp. 6243–6250. II-D
- [35] C.-X. Ren, Y.-H. Liu, X.-W. Zhang, and K.-K. Huang, "Multi-source unsupervised domain adaptation via pseudo target domain," *IEEE Transactions on Image Processing*, vol. 31, pp. 2122–2135, 2022. II-D
- [36] X. Mao, Q. Li, H. Xie, R. Y. Lau, Z. Wang, and S. Paul Smolley, "Least squares generative adversarial networks," in *Proceedings of the IEEE international conference on computer vision*, 2017, pp. 2794–2802. II-D
- [37] Anonymous, "Domain generalization with small data," in *Submitted to The Eleventh International Conference on Learning Representations, 2023*, under review. [Online]. Available: <https://openreview.net/forum?id=RKiWwhocuiU> II-E
- [38] J.-Y. Zhu, T. Park, P. Isola, and A. A. Efros, "Unpaired image-to-image translation using cycle-consistent adversarial networks," in *Proceedings of the IEEE international conference on computer vision*, 2017, pp. 2223–2232. II-E, III-C, III-C
- [39] J. Johnson, A. Alahi, and L. Fei-Fei, "Perceptual losses for real-time style transfer and super-resolution," in *European conference on computer vision*. Springer, 2016, pp. 694–711. II-E
- [40] A. Graves, "Practical variational inference for neural networks," *Advances in neural information processing systems*, vol. 24, 2011. III-B
- [41] R. Krishnan, M. Subedar, and O. Tickoo, "Specifying weight priors in bayesian deep neural networks with empirical bayes," in *AAAI*, vol. 34, no. 04, 2020, pp. 4477–4484. III-B
- [42] K. Dabov, A. Foi, V. Katkovnik, and K. Egiazarian, "Image denoising with block-matching and 3d filtering," in *Image processing: algorithms and systems, neural networks, and machine learning*, vol. 6064. SPIE, 2006, pp. 354–365. III-C
- [43] Z. S. Kelm, D. Blezek, B. Bartholmai, and B. J. Erickson, "Optimizing non-local means for denoising low dose ct," in *2009 IEEE International Symposium on Biomedical Imaging: From Nano to Macro*. IEEE, 2009, pp. 662–665. III-C
- [44] N. Moran, D. Schmidt, Y. Zhong, and P. Coady, "Noisier2noise: Learning to denoise from unpaired noisy data," in *Proceedings of the IEEE/CVF Conference on Computer Vision and Pattern Recognition*, 2020, pp. 12064–12072. III-C
- [45] M.-H. Laves, M. Tolle, A. Schlaefer, and S. Engelhardt, "Posterior temperature optimized bayesian models for inverse problems in medical imaging," *Medical Image Analysis*, vol. 78, 2022. III-C
- [46] Z. Wang, A. C. Bovik, H. R. Sheikh, and E. P. Simoncelli, "Image quality assessment: from error visibility to structural similarity," *IEEE transactions on image processing*, vol. 13, no. 4, pp. 600–612, 2004. III-C
- [47] W. Xue, L. Zhang, X. Mou, and A. C. Bovik, "Gradient magnitude similarity deviation: A highly efficient perceptual image quality index," *IEEE transactions on image processing*, vol. 23, no. 2, pp. 684–695, 2013. III-C
- [48] L. Zhang and H. Li, "Sr-sim: A fast and high performance iqa index based on spectral residual," in *2012 19th IEEE international conference on image processing*. IEEE, 2012, pp. 1473–1476. III-C